

Manipulation of magnetic-flux landscapes in superconducting $\text{Bi}_2\text{Sr}_2\text{CaCu}_2\text{O}_{8+\delta}$ crystals

D. COLE¹, S. J. BENDING¹, S. SAVEL'EV^{2,3}, T. TAMEGAI⁴ and FRANCO NORI^{2,5}

¹ *Department of Physics, University of Bath - Claverton Down, Bath, BA2 7AY, UK*

² *Frontier Research System, The Institute of Physical and Chemical Research (RIKEN) Wako-shi, Saitama, 351-0198, Japan*

³ *Department of Physics, Loughborough University - Loughborough LE11 3TU, UK*

⁴ *Department of Applied Physics, The University of Tokyo - 7-3-1 Hongo Bunkyo-ku, Tokyo - 113-8656, Japan*

⁵ *Center for Theoretical Physics, Department of Physics, University of Michigan Ann Arbor, MI, 48109-1040, USA*

received 26 June 2006; accepted in final form 31 October 2006

published online 1 December 2006

PACS. 74.25.Qt – Vortex lattices, flux pinning, flux creep.

PACS. 74.72.Hs – Bi-based cuprates.

Abstract. – We demonstrate experimentally that the micromagnetic profile of the out-of-plane component of magnetic induction of layered superconductors, B_z , can be manipulated by varying the in-plane magnetic field, H_{\parallel} . Moving Josephson vortices, confined between layers, drag pancake vortex stacks carrying out-of-plane flux, and the magnetic profile, $B_z(x)$, can be controllably shaped across the entire sample. Depending on the magnetic history and temperature we can increase or decrease the out-of-plane flux density at the center and near the edges of the crystal by as much as $\sim 40\%$, realising both “convex and concave magnetic flux lenses”. Our experimental results are well described by molecular dynamics simulations.

Introduction. – In recent years dramatic progress has been made in the control of critical currents in superconducting films by the introduction of arrays of artificial vortex pinning sites (*e.g.*, antidots or ferromagnetic dots) [1–4]. The next major challenge is to control *local* vortex densities, so that different flux profiles can be realised in the same superconducting sample. The ability to manipulate vortices at will could, for example, allow one to remove flux noise sources from sensitive superconducting devices, *e.g.*, SQUID magnetometers or qubits, and greatly improve their performance. Strategies to achieve vortex control have recently been proposed [5] and demonstrated [6–10] in so-called “ratchet devices” which incorporate a spatially asymmetric nanoscale ratchet potential to achieve rectification of ac drives. Alternative approaches have been proposed for motion control in binary mixtures of interacting particles where one component is dragged by another [11]. A specific implementation of this scheme has been described to develop vortex-pumps, vortex-diodes and vortex-lenses in highly anisotropic layered superconductors under tilted magnetic fields [12]. We recently realised a vortex lens in $\text{Bi}_2\text{Sr}_2\text{CaCu}_2\text{O}_{8+\delta}$ (BSCCO) experimentally [13] by exploiting the response of crossing vortex

lattices to trains of time-asymmetric in-plane field pulses. These devices [13] operate far from equilibrium, and control the lensing amplitude by varying the shape/frequency of the field pulses, temperature and out-of-plane magnetic field component. In contrast, we now describe the experimental realisation of a flux lens which works in a completely different limit when the vortex system is perturbed via *adiabatic* changes of the external conditions. Even though we do not deliberately break any symmetries of our system, we show that it is still possible to use the vortex dragging phenomenon to achieve very large lensing and antilensing effects. Here the term “lens” has been coined to describe the situation in which the vortex density is enhanced in a given region of the sample (the analog of a convex optical lens), while “antilens” refers to vortex depletion (\equiv concave lens). We make a detailed investigation of the dependence of adiabatic lensing on the position in the crystal, pancake vortex density and temperature, and present a molecular dynamics model which accurately reproduces all the main features of our data.

Direct visualization [14–19] has revealed that a tilted (away from the crystalline c -axis) magnetic field penetrates the highly anisotropic BSCCO superconductor in two interpenetrating vortex arrays, known as crossing vortex lattices [20, 21]. One vortex sublattice consists of stacks of pancake vortices (PVs) aligned along the c -axis, while the other sublattice is formed by Josephson vortices (JVs) confined between CuO_2 layers. Superconducting currents generated by JVs deform stacks of PVs, resulting in a mutual attraction between PVs and JVs [21, 22]. This has been experimentally confirmed [14–16] by the observation of PV chains which decorate underlying JV stacks in tilted magnetic fields. For low out-of-plane field components, $H_z(\text{Oe}) < 0.2\sqrt{H_{\parallel}(\text{Oe})}$, where H_{\parallel} is the component parallel to the CuO_2 planes, all PVs are trapped on underlying Josephson vortices in the so-called “chain state” [17]. For larger values of H_z these chains coexist with a reasonably well ordered lattice of free PVs in the mixed chains/lattice state. JVs are usually very weakly pinned and, at equilibrium, form a highly elongated rhombic lattice. JVs can be moved by changing the in-plane magnetic field component, H_{\parallel} (*i.e.* by deforming the JV lattice), and the moving JVs drag PVs along with them [23].

Experimental results. – Our vortex lensing experiments have been performed on an as-grown BSCCO superconducting single crystal ($T_c = 91$ K, dimensions $1 \text{ mm} \times 0.75 \text{ mm} \times 50 \mu\text{m}$). The changes in B_z arising from PV lensing/antilensing were detected by mounting the crystal on a $25 \mu\text{m}$ wirewidth micro-Hall probe array patterned in a GaAs/AlGaAs 2D electron gas [24]. The dimensions of the active areas of the array were small enough to give adequate spatial resolution across the BSCCO single crystal, but large enough to average out mesoscopic signals due to discrete PV chains passing above it. The array has thirteen addressable elements, of which twelve were situated at different positions under the crystal and the remaining uncovered one acted as a reference. The sensor was driven by a $45 \mu\text{A}$ 32 Hz ac current and the Hall voltages detected with a lock-in amplifier. The out-of-plane (H_z) and in-plane (H_{\parallel}) magnetic field components are varied independently using a solenoid and Helmholtz coil pair (one of which could be precisely positioned vertically on a micrometer driven stage), respectively. The latter is adjusted to align the in-plane field component to within $\pm 0.006^\circ$ of the ab crystallographic planes, using the in-plane “lock-in” transition [13, 25] as an alignment signature. This corresponds to the generation of supercurrents within the crystal which completely screen the out-of-plane component of applied magnetic field. At sufficiently high temperatures lock-in only occurs for very small misalignment angles, yielding a very sensitive indication. At the start of lensing experiments a fixed PV density was established by field-cooling the BSCCO crystal from above T_c in a known value of the out-of-plane field, H_z . The in-plane magnetic field, H_{\parallel} , was then cycled several times until a reproducible steady-state

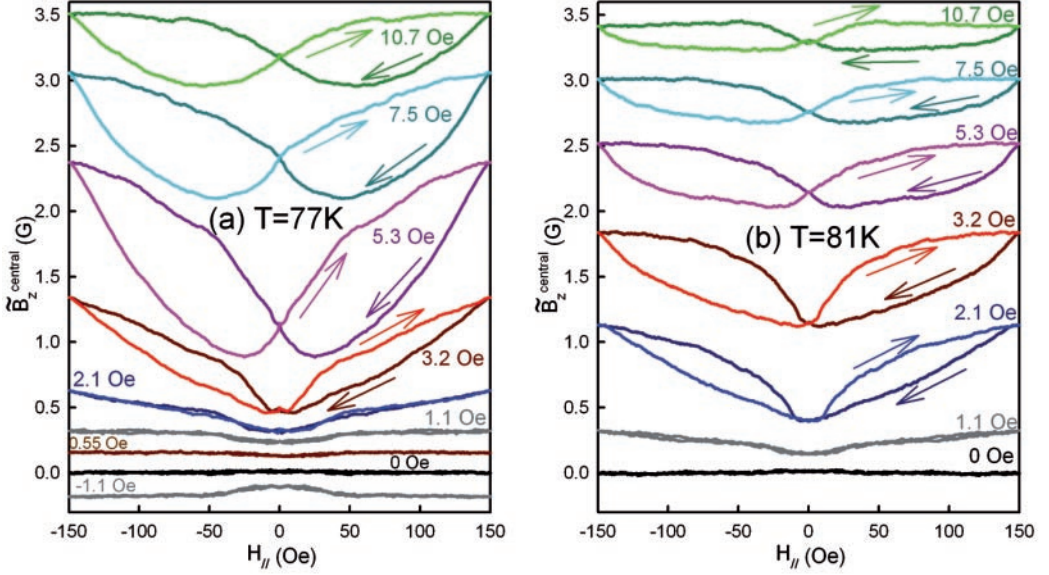


Fig. 1 – (Color online) The local out-of-plane magnetic induction, \tilde{B}_z , (vertically offset for clarity) *vs.* the in-plane magnetic field, H_{\parallel} , measured near the center of the sample at (a) 77 K and (b) 81 K. Arrows indicate the direction of the H_{\parallel} field sweep.

loop was obtained. During each cycle, H_{\parallel} was slowly ramped (1.7 Oe s^{-1}) up to a maximum of 150 Oe and down to a minimum of -150 Oe and back to zero, while the Hall voltage was monitored at a chosen array element to measure the magnetic induction, B_z . Note that this sweep rate is more than two orders of magnitude smaller than those used to achieve “conditioning” of the pancake vortex system in the non-equilibrium experiments of ref. [13]. Hence we are working in a limit where the frequency dependence of JV/PV coupling, the PV viscosity and the response time of the JV lattice play no role. In practice these “work hardened” traces were still not completely symmetric, even after precise H_{\parallel} alignment, due to the fact that the crystal and Hall probe are not exactly co-planar. To account for this the presented data have been symmetrized: $\tilde{B}_z \uparrow (H_{\parallel}) = \tilde{B}_z \downarrow (-H_{\parallel}) = \frac{1}{2}[B_z \uparrow (H_{\parallel}) + B_z \downarrow (-H_{\parallel})]$.

The observed lensing response was a strong function of the measurement position across the crystal. For the sake of brevity, we only present data for two elements which fully illustrate the extremes of behaviour seen, one at the sample center and one near the edge ($225\ \mu\text{m}$ from one of the edges parallel to H_{\parallel}). Figures 1 and 2 show *changes* of \tilde{B}_z as a function of H_{\parallel} measured at the central location and near the edge of the sample, respectively, for various values of H_z . In both cases for $H_z < 2\text{ Oe}$ (chains regime), the PV system shows a weak reversible response which inverts when H_z changes sign, attributable to the dragging of PV stacks which are *all* trapped on JV chains. For $H_z > 2\text{ Oe}$ (mixed chains/lattice regime), free PVs exist between chains and we start to see stronger, irreversible behaviour related to the compression of untrapped PVs, and their cutting through JV stacks at high in-plane fields.

Sample center. – At $T = 77\text{ K}$ and high H_z the magnetic induction loop $\tilde{B}_z(H_{\parallel})$ for the central element (fig. 1a) has a “butterfly” shape exhibiting: i) a fast increase of PV density when H_{\parallel} increases from zero, followed by a weaker (saturation-like) dependence of $\tilde{B}_z^{\text{central}}(H_{\parallel})$; ii) a rapid reduction of $\tilde{B}_z^{\text{central}}(H_{\parallel})$ when H_{\parallel} decreases from its maximum

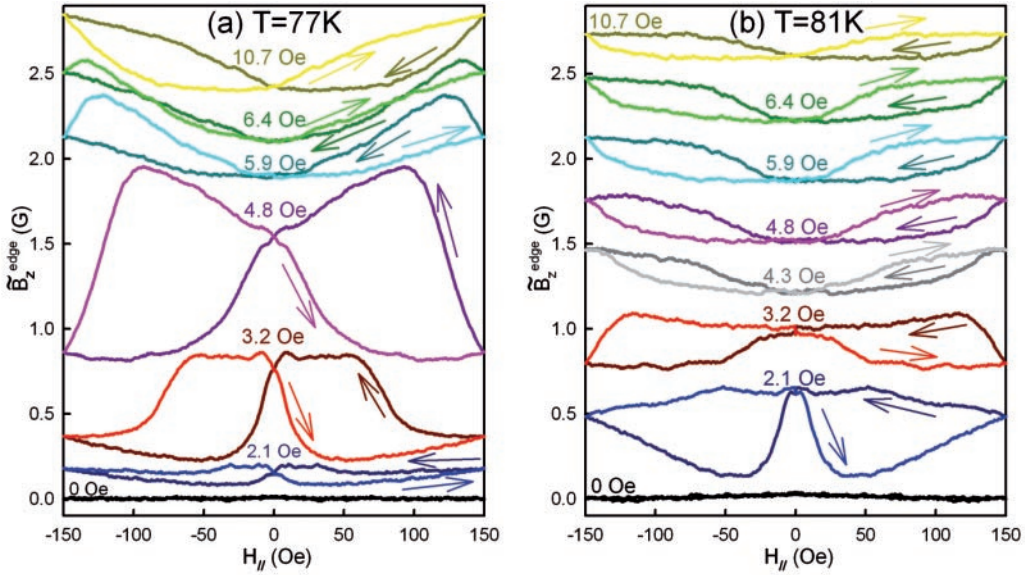


Fig. 2 – (Color online) The local out-of-plane magnetic induction, \tilde{B}_z , (vertically offset for clarity) *vs.* the in-plane magnetic field, H_{\parallel} , measured near the edge of the sample at (a) 77 K and (b) 81 K. Arrows indicate the direction of the H_{\parallel} field sweep.

value, followed by a remarkable *antileensing* (an overshoot in the reduction of PV density) effect $\tilde{B}_z^{\text{central}} \downarrow (H_{\parallel} > 0) < \tilde{B}_z^{\text{central}}(H_{\parallel} = 0)$. Similar, but weaker, lensing behaviour is seen at 81 K (fig. 1b). The maximum lensing effect now occurs at a lower value of H_z due to a small decrease in JV/PV coupling strength and increased PV-PV repulsion due to the longer PV penetration depth at higher temperatures.

At 77 K the experimental lensing efficiency, defined as $\left(\max \left[\tilde{B}_z^{\text{central}}(H_{\parallel}) \right] - \min \left[\tilde{B}_z^{\text{central}}(H_{\parallel}) \right] \right) / \tilde{B}_z^{\text{central}}(H_{\parallel} = 0) \times 100\%$ exhibits a maximum of nearly 40% at $H_z \sim 5$ Oe. Empirically we observe the maximum lensing efficiency near 70 K. At this temperature the pinning strength is optimal, being large enough to prevent “compressed” PVs from escaping sideways parallel to JVs, but not so strong that the dragging of PVs by JVs is completely suppressed. Note that on the H_{\parallel} -increasing branch of the lensing loop, $\tilde{B}_z^{\text{central}}(H_{\parallel})$ is always higher than the decreasing branch, *i.e.*, $\tilde{B}_z^{\text{central}} \uparrow (H_{\parallel}) > \tilde{B}_z^{\text{central}} \downarrow (H_{\parallel})$. We denote such loops as “clockwise”, when considering the right-side ($H_{\parallel} > 0$) of the hysteresis cycle.

Sample edge. – The data, $\tilde{B}_z^{\text{edge}}$, from the Hall element near the sample edge (fig. 2) provide insights into the spatial distribution of the PV density in our lensing experiments. In stark contrast to fig. 1, we now see strong antileensing behaviour for $2\text{ Oe} < H_z < 4.8\text{ Oe}$ at 77 K (fig. 2a), and $2\text{ Oe} < H_z < 3.2\text{ Oe}$ at 81 K (fig. 2b). This is easily understood in terms of the PV profiles generated during our experiments. Since PVs are pushed from two opposite edges of the sample towards the center, there must be regions near these edges which experience a decrease in PV density, while accumulation is occurring in the crystal center (see sketched profiles in fig. 3). It is interesting to note that the counter-clockwise loops, $\tilde{B}_z^{\text{edge}} \uparrow (H_{\parallel}) < \tilde{B}_z^{\text{edge}} \downarrow (H_{\parallel})$, at low H_z transform into clockwise ones when H_z increases above 6.4 Oe for $T = 77\text{ K}$. This is best illustrated in the curve at $H_z = 6.4\text{ Oe}$, which shows

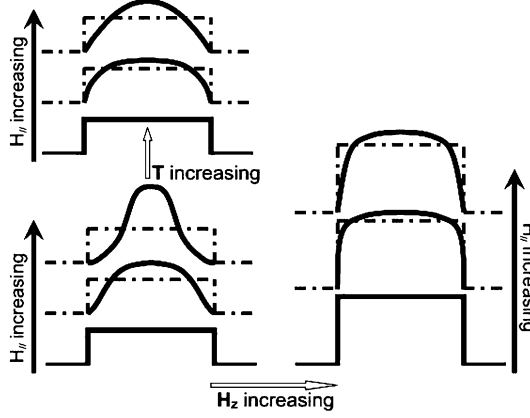


Fig. 3 – Sketches of PV density profiles across the crystal for increasing H_{\parallel} (bottom to top). The three different panels illustrate how the profiles vary as the temperature and H_z are increased.

two crossing points for $H_{\parallel} > 0$ between traces on the sweep-up and sweep-down. At such high values of H_z PVs penetrating through the sample surface partially compensate for the deficit of PVs near the edges, and enhanced PV-PV repulsion results in a broadening of the focus region and a shift of the lensing/antilinging interface towards the sample edge. Hence a transition from counter-clockwise to clockwise $\tilde{B}_z^{\text{edge}}$ loops occurs as the out-of-plane field is increased. Comparison of figs. 2a, b also reveals that the crossover from anticlockwise to clockwise loops occurs for lower values of H_z at higher temperatures. This is what one would intuitively expect since the longer PV penetration depth at higher temperatures will lead to stronger PV-PV repulsion (relative to the PV/JV attraction) and a broadening of the lensing/antilinging profiles. These effects are illustrated qualitatively in fig. 3. Note that the maximum antilinging effect also shifts to lower H_z at higher temperature, due again to slightly decreased JV/PV coupling strength and increased PV-PV repulsion.

Flux profiles in BSCCO crystals can be dominated by geometrical barriers at high temperatures [26]. Our simulations and preliminary magneto-optical studies reveal that the discussed lensing effect is partially suppressed due to competition with the so-called *vortex dome* (accumulation of PVs at the sample center) at high fields (above the vortex penetration field) if the geometrical barrier is high enough.

Simulations. – All features of the dc vortex lenses discussed above can be qualitatively captured by a simple model describing the motion of interacting PVs and JVs [13]:

$$\eta_J \dot{x}_i^J / b^J = f_i^{JJ} + f_i^{JH} + f_i^{JP}, \quad \eta_P \dot{x}_k^P / a^P = f_k^{PP} + f_k^{PH} + f_k^{PJ}, \quad (1)$$

where x_i^J and x_k^P are the positions of JV and PV rows with distances b^J and a^P between JVs and PVs in a row, respectively, the dot on top of x_i denotes the time derivative, while η_J and η_P are the JV and PV viscosities per unit length. The viscous forces slowing down the vortex motion are balanced by: 1) the repulsive force f^{JJ} between JV rows (including images of rows with respect to the sample surface); 2) the interaction f^{JH} of JV rows with Meissner currents generated by the externally applied magnetic field H_{\parallel} ; 3) the repulsion f^{PP} between PV rows (including images); 4) the interaction f^{PH} of PV rows with H_z ; and 5) the “crossing lattices” attractive forces f^{JP} between rows of JVs and PVs. Further details of the simulation procedure as well as the parameters used can be found in ref. [13].

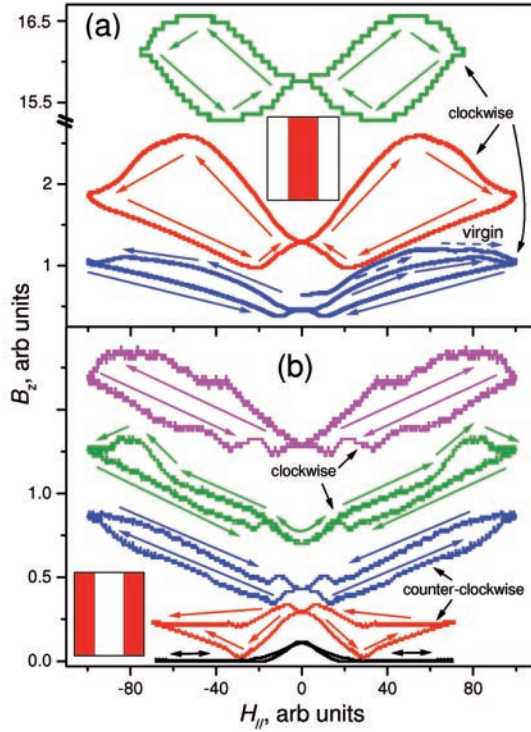


Fig. 4 – (Color online) Simulated loops of the local induction $B_z(H_{\parallel})$ (a) at the center and (b) near the sample edges for different values of H_z (H_z increasing from bottom to top in each panel). The red region in each inset indicates where B_z was monitored in the sample. The main features found in experiments (figs. 1, 2) are reproduced in the simulations.

The results of the simulations (*e.g.*, in fig. 4, color online) are in good qualitative agreement with the experimental data at the sample center: i) First, B_z^{central} increases with H_{\parallel} (fig. 4a), as JVs move towards the sample center and drag PVs with them. This is consistent with theoretical predictions [12]; ii) At a certain in-plane field H_{\parallel} , the PV density at the center of the sample saturates and even starts to decrease. The PV density at the center is now large enough that PV-PV repulsion becomes dominant. Thus, PVs start to cut through the JV rows; iii) On the decreasing branch of the loop, both experiments and simulations exhibit a remarkable antilensing effect (see animations in [27]). This arises because a smaller total number of PVs now spreads out over the whole sample, resulting in a deficit of PVs at the center, *i.e.*, a decrease of B_z^{central} below its initial value when $H_{\parallel} = 0$. Also the ratio of the lensing to antilensing effect, $\max[B_z^{\text{central}}(H_{\parallel}) - B_z^{\text{central}}(0)] / |\min[B_z^{\text{central}}(H_{\parallel}) - B_z^{\text{central}}(0)]|$ decreases to about one when the out-of-plane field increases, in agreement with experiments (this produces rounder loops for higher H_z , see figs. 1a, b and 4a). The simulations also capture the main features found in the experiments near the sample edge (see fig. 4b): i) At low out-of-plane fields, H_z , counter-clockwise loops are calculated, whose area *increases* with H_z (changing from the black curve to the red one); ii) at higher out-of-plane fields the counter-clockwise loops *narrow* (changing from the red curve to the blue one), transform into clockwise loops (changing from the blue curve to the green one) and *broaden* again (changing from the green curve to the magenta one).

Conclusions. – We have experimentally realized magnetic vortex “lenses” which controllably focus and defocus the out-of-plane magnetic flux in a $\text{Bi}_2\text{Sr}_2\text{CaCu}_2\text{O}_{8+\delta}$ sample. Remarkably, this was achieved by exploiting the adiabatic “dragging” of PVs by JVs without deliberately breaking spatial or temporal symmetries in the sample. The PV density near the center/edges of the sample can readily be controlled by changing either the in-plane or the mean out-of-plane magnetic field components, as well as the temperature. Our experimental results are well described by a simple model considering the dragging of one vortex species by the other. This novel method of vortex motion control opens up new avenues for the manipulation of flux quanta and nanoscale particles.

* * *

We acknowledge support from EPSRC in the UK under grant No. GR/R46489/01, EPSRC Advanced Research Fellowship No. D072581/1, the ESF VORTEX and AQDJJ networks, the US NSA, LPS, ARO, NSF grant No. EIA-0130383, and the Grant-in-Aid No. 18740224 from MEXT, Japan.

REFERENCES

- [1] BAERT M. *et al.*, *Phys. Rev. Lett.*, **74** (1995) 3269.
- [2] MARTIN J. I. *et al.*, *Phys. Rev. Lett.*, **79** (1997) 1929.
- [3] MORGAN D. J. *et al.*, *Phys. Rev. Lett.*, **80** (1998) 3614.
- [4] VAN BAEL M. J. *et al.*, *Phys. Rev. B*, **68** (2003) 014509.
- [5] LEE C.-S. *et al.*, *Nature*, **400** (1999) 337; WAMBAUGH J. F. *et al.*, *Phys. Rev. Lett.*, **83** (1999) 5106; OLSON C. J. *et al.*, *Phys. Rev. Lett.*, **87** (2001) 177002; ZHU B. Y. *et al.*, **92** (2004) 180602.
- [6] KWOK W. K. *et al.*, *Physica C*, **382** (2002) 137.
- [7] VILLEGAS J. E. *et al.*, *Science*, **302** (2003) 1188.
- [8] VAN DE VONDEL J. *et al.*, *Phys. Rev. Lett.*, **94** (2005) 057003; DE SOUZA SILVA C. C. *et al.*, *Nature*, **440** (2006) 651; NORI F., *Nat. Phys.*, **2** (2006) 227.
- [9] TOGAWA Y. *et al.*, *Phys. Rev. Lett.*, **95** (2005) 087002.
- [10] WÖRDENWEBER R. *et al.*, *Phys. Rev. B*, **69** (2004) 184504.
- [11] SAVEL'EV S. *et al.*, *Phys. Rev. Lett.*, **92** (2004) 160602; **91** (2003) 010601; SAVEL'EV S. *et al.*, *Chaos*, **15** (2005) 026112.
- [12] SAVEL'EV S. and NORI F., *Nat. Mater.*, **1** (2002) 179.
- [13] COLE D., BENDING S., SAVEL'EV S., GRIGORENKO A., TAMEGAI T. and NORI F., *Nat. Mater.*, **5** (2006) 305; TONOMURA A., *Nat. Mater.*, **5** (2006) 257.
- [14] MATSUDA T. *et al.*, *Science*, **294** (2001) 2136.
- [15] GRIGORENKO A. *et al.*, *Nature*, **414** (2001) 728.
- [16] VLASKO-VLASOV V. K. *et al.*, *Phys. Rev. B*, **66** (2002) 014523.
- [17] BENDING S. J. *et al.*, *Physica C*, **412-414** (2004) 372.
- [18] TOKUNAGA M. *et al.*, *Phys. Rev. B*, **66** (2002) 060507(R).
- [19] BOLLE C. A. *et al.*, *Phys. Rev. Lett.*, **66** (1991) 112.
- [20] BULAEVSKII L. N. *et al.*, *Phys. Rev. B*, **46** (1992) 366.
- [21] KOSHELEV A. E., *Phys. Rev. Lett.*, **83** (1999) 187.
- [22] SAVEL'EV S. E. *et al.*, *Phys. Rev. B*, **64** (2001) 094521.
- [23] PERKINS G. K. *et al.*, *Supercond. Sci. Technol.*, **18** (2005) 1290.
- [24] JAMES M. S. *et al.*, *Phys. Rev. B*, **56** (1997) R5771.
- [25] KOSHELEV A. E., *Phys. Rev. B*, **48** (1993) 1180.
- [26] ZELDOV E. *et al.*, *Phys. Rev. Lett.*, **73** (1994) 1428.
- [27] Animations illustrating vortex lensing are available at <http://dml.riken.go.jp/vortex-dc>.